

A NOVEL ALTERNATIVE IN WIRELESS AND PASSIVE SENSING: THE BENDED NESTED SPLIT-RING RESONATOR

Burak OZBEY¹

¹Department of Electrical and Electronics Engineering, Ankara University,
Ankara, TÜRKİYE

ABSTRACT. In this paper, a new split-ring resonator variant, called the bended nested split-ring resonator (B-NSRR) is introduced. B-NSRR is a modified version of the nested split-ring resonator (NSRR) geometry, which has been successfully utilized in sensing of various physical quantities such as strain, displacement and moisture content due to its superior sensitivity, resolution and compactness in comparison to more traditional structures such as SRR and electrical SRR (ESRR). The B-NSRR geometry is demonstrated to allow an even more compact structure, while retaining the high sensitivity level of the NSRR. The performances obtained by the SRR, ESRR, NSRR and B-NSRR geometries are compared for displacement and moisture content sensing applications. Simulations are carried out to validate the findings, where modified versions of SRR-based structures are employed as displacement sensors and a comparison is made between their performances. Owing to its compactness and high sensitivity, it is shown that the B-NSRR is a reasonable alternative to available geometries in various sensing applications.

1. INTRODUCTION

Metamaterials are periodic structures which can be used to generate exotic behavior that cannot be achieved by natural materials. The interesting phenomena that have been proposed and/or demonstrated include left-handed materials with negative effective permittivity and permeability [1–3], superlenses [4], zero-index ultradirective materials [5], artificial magnetic conductors [6] and electromagnetic cloaks [7]. The potential of metamaterials and frequency-selective surfaces (FSS) in diverse areas has also motivated researchers to apply these results to well-known engineering problems to come up with novel superior designs. Examples of metamaterial-based structures in antenna and microwave engineering include thin sub-wavelength cavity resonators [8], phase shifters which can produce positive, negative or 0 phase shifts while maintaining the same short overall length [9], compact stopband filters [10],

Keywords. Split-ring resonator (SRR), nested split-ring resonator (NSRR), wireless sensor, passive sensor, displacement sensor, moisture content sensor, microwave sensing.

 ozbey@ankara.edu.tr-Corresponding author;  0000-0001-7485-2132.

broadband baluns [11], electrically-small antennas with increased radiation [12], and many more. Metamaterials can also be employed to generate a strong localization and enhancement of electromagnetic fields, which in turn can be used to obtain ultrasensitive and high-resolution sensor designs for detection of many different stimuli [13]. Metamaterial-based sensors that have been proposed in literature include a long-list of works, among which biosensors [14], thin-film sensors [15], strain sensors [16] pressure sensors [17, 18] and temperature sensors [18] can be cited.

Since their theoretical introduction in [19], the building blocks of metamaterials have been the split-ring resonator (SRR). A single SRR is a small-loop antenna, which leads to negative magnetic polarization and effective permeability due to cancellation of the incident field and the out-of-phase locally-scattered field 20 when operated at a slightly higher frequency. When the structure is used as a unit cell in two dimensional repeating patterns, the resulting SRR array acts as a μ -negative metamaterial, where μ is the magnetic permeability. The single structure, on the other hand, is useful by itself as a sensor, because of its high field localization. The SRR can be visualized as an LC resonator, whose capacitance can be increased by introducing additional rings of different total metal length. A variant of SRRs, called the electric split-ring resonator (ESRR) was introduced in [21]. Contrary to the SRR, this structure produces little or no response to magnetic field illumination, but exhibits strong sub-wavelength resonance characteristics to the incident electric field. In addition to numerous other SRR variants, both the original SRR and ESRR have been widely used as a sensor in their single structure form, due to their high sensitivity. Despite having been very popular in sensing applications, these structures have drawbacks. The most important of these is that the SRR and the ESRR structures do not enable designs which are compact enough. Compactness is critical in applications such as biosensing, where in vivo measurement of vital signs requires small structures. In addition, many biosensing applications dictate a relatively low frequency in order to avoid the background absorption that takes place in the soft tissue. In some other sensing applications, most prominently for the radio frequency identification (RFID)-based tags in antenna form, increasing the operation frequency leads to increased loss and lower sensitivity [22]. Therefore, it is important to have a compact design which allows for both low frequency operation and high sensitivity. For this purpose, a new SRR variant, called the nested split-ring resonator (NSRR) was proposed in [23], where it was demonstrated by experiments that the NSRR enables a much more compact footprint compared to classic SRR, as well as a higher sensitivity. The NSRR geometry is shown in Figure 1(a). Originally intended as a biological strain sensor to evaluate the progression of long-bone fracture healing [23], the NSRR structure has also been exploited in sensing critical damage parameters such as displacement [24–28] and two-dimensional average strain [29, 30] in civil engineering structures, as well as in biological applications to sense the moisture content in plants [31]. The NSRR structure has proven

to be a useful alternative since it offers a non-destructive, wireless and passive method which also demonstrates a high sensitivity and resolution.

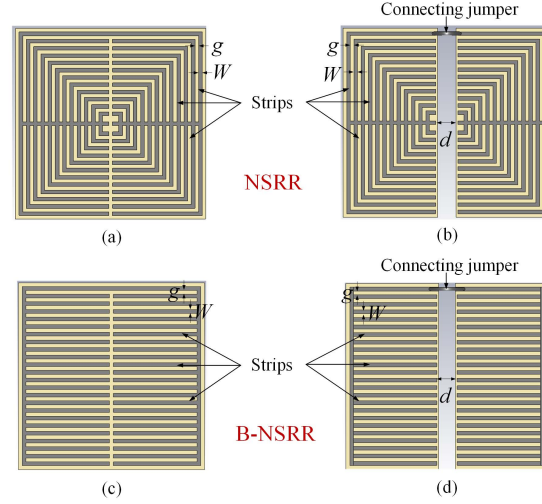


FIGURE 1. (a) Nested split-ring resonator (NSRR) geometry, (b) Modified NSRR geometry for displacement sensing, (c) Bended nested split-ring resonator (B-NSRR) geometry, (d) Modified B-NSRR geometry for displacement sensing.

In this work, we propose a novel NSRR-based sub-wavelength resonating structure, called the bended nested split-ring resonator (B-NSRR). The geometry of B-NSRR is shown in Figure 1(c). It includes a high number of thin coplanar metallic strips similar to the NSRR, however, the strips are not of the same size as in the NSRR, but of linearly decreasing length towards the center, making a 90° bend at the corners. This geometry increases the coplanar capacitance in comparison to the NSRR, while keeping the gap capacitance between opposing strips the same. This effect is especially pronounced when the number of strips is increased. Thus, the total capacitance is enhanced, which makes way for even a more compact design. As a variant of the NSRR, B-NSRR can be utilized in various sensing applications. Two of them, relative displacement sensing and moisture content sensing are demonstrated in this paper with full-wave electromagnetic simulations, where the change of the sensor resonance frequency is tracked versus monitored quantity. The sensing performances of the classic SRR, ESRR, NSRR and B-NSRR are compared for structures having approximately the same resonance frequency. The organization of this work is as follows: In Section 2, the B-NSRR geometry is discussed in terms of the NSRR and its equivalent circuit model. In Section 3, full-wave electromagnetic simulations of the four principal SRR geometries are presented for

wireless relative displacement and moisture content sensing. Section 4 concludes the paper.

2. THE B-NSRR GEOMETRY

2.1. NSRR Geometry and Its Equivalent Circuit Model. B-NSRR is a variant of the the NSRR geometry, which is shown in Figure 1(a). The NSRR consists of a number of opposing metallic strip pairs with a gap in between, which are aligned in vertical direction on a dielectric substrate. They are connected from the other end to a continuous uppermost strip, which makes the structure a combination of split-rings of different lengths which are connected in parallel. When the number of these “nested” split-rings, N , is relatively high, the capacitances coming from each split-ring is therefore added to yield a high capacitance value. The equivalent circuit model of the NSRR geometry is presented in Figure 2. The structure can be visualized as an LC resonator [32], where the inductance L_s is proportional to the length of each strip, while the capacitance has two forms: 1) The gap capacitance C_{gap} between each opposing strip, and 2) the capacitance between two parallel strips C_s [32]. The increase of both C_s and C_{gap} due to a high N in NSRR geometry increases the overall capacitance, which in turn leads to a decreased resonance frequency f_{res} , since $f_{res} = 1/\sqrt{L_{eff}C_{eff}}$, where L_{eff} and C_{eff} are the overall NSRR inductance and capacitance, respectively. For a given wavelength, increasing N thus allows for a more compact design in comparison to structures such as the SRR or the ESRR. The structure in this form can be used to measure physical quantities, which are correlated with electrical parameters of the medium. For instance, moisture content of the material on which the NSRR can be attached, or, the relative humidity of the medium can be measured, since variation of the water content in the material or in the air leads to a change in complex permittivity ϵ_r , which in turn affects C_{eff} . Likewise, mechanical changes on the NSRR structure also lead to a change in its electrical parameters. For example, strain induced on the NSRR is highly correlated with f_{res} , since it elongates or contracts the structure, which in turn changes C_{eff} and L_{eff} . Similarly, formation of a crack either on the medium behind the NSRR sensor or on the sensor itself, changes the electrical characteristics of the system. In order to measure relative displacement between two points, the NSRR structure can be split vertically into two symmetric halves, as shown in Figure 1(b). This way the halves become mechanically-independent. In order to maintain the electrical connection of the uppermost strip, the two halves are shorted by a thin jumper. This way, each NSRR half can be point-attached to a material under test, and if a displacement occurs between the two attachment points, this changes the gap d between the two structures. The variation of d is correlated with f_{res} , and by a calibration, it is possible to extract d wirelessly from the measurement of f_{res} [24]. It is possible to use either a one-channel measurement setup, where a transceiver antenna forms a coupled system with the NSRR, or, a two channel system where two antennas are

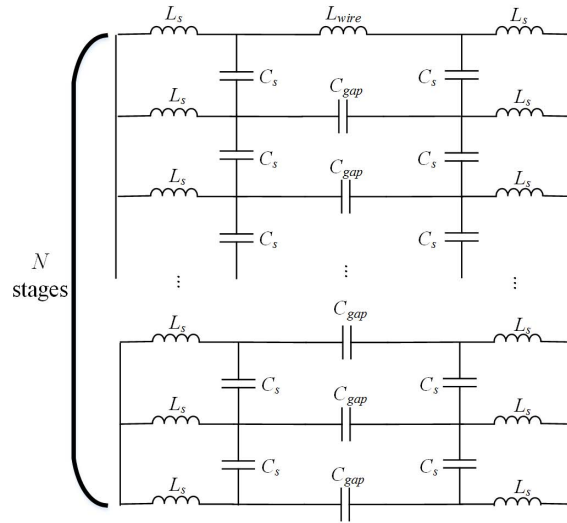


FIGURE 2. Equivalent circuit model of the NSRR geometry [32].

used where one of them sends a TX signal and the other receives the backscattered wave. In the first configuration, the NSRR resonance can be tracked directly from the spectrum of the transceiver antenna, but the interrogation distance is limited to near-field of the antenna [24, 27]. In the second configuration, it has been shown that the TX antenna can be taken to far field, but the RX antenna still has to be at a close distance [28] to maintain the high levels of sensitivity and resolution. In terms of the equivalent circuit model, the shorting wire brings an additional inductance, denoted as L_{wire} , which is in series with the uppermost strip as shown in Figure 2. The inclusion of the wire in the modified NSRR makes the geometry sensitive to magnetic field illumination. Normally a capacitance-dominated structure, only a horizontally polarized electric field is able to induce surface currents on the classic NSRR geometry. In the modified form, the jumper acts a magnetic loop to couple with incident magnetic fields, as well. How the resonance frequency shift occurs when the NSRR or the modified NSRR structure is employed as a sensor depends on the type of the sensing application. For example, for a strain or displacement sensor, the parameter d becomes subject to change, and therefore the dominating change occurs in the gap capacitance C_{gap} . On the other hand, for a moisture content sensor, an additional capacitance is brought in by the changing electrical properties of the medium.

2.2. Characteristics of the B-NSRR Geometry. Similar to the NSRR geometry, the proposed B-NSRR geometry also incorporates a high number of strips

to increase the overall capacitance. In essence, the field localization mechanism is very similar to the NSRR, since both geometries consist of nested split-rings which present parallel capacitances between the parallel and the opposing strips. Furthermore, the gap capacitance C_{gap} is also the same for both geometries, which is important in retaining the high sensitivity (as high 13 MHz/mm) and resolution ($\sim 1\mu\text{m}$) levels obtained in displacement sensing [24,28]. However, differently from the NSRR, the B-NSRR does not have a fixed strip length. Therefore, the strip inductance L_s and the parallel strip capacitance C_s do have a fixed value, but they change while moving from the center towards the top and the bottom of the structure. Here, the innermost strip produces the smallest L_s and C_s . On the other hand, the outermost strip produces the greatest L_s and C_s , which are around twice that are obtained by the NSRR structure, since the strip inductance and capacitance are linearly proportional to the length of the strip. Therefore, when the number of strips N is relatively small, the B-NSRR geometry is expected to generate a higher total capacitance and inductance. Here, the total parallel strip length is defined as the sum of each path length passing through the midsection of a neighboring parallel strip pair, as shown in Figure 3 with dashed lines.

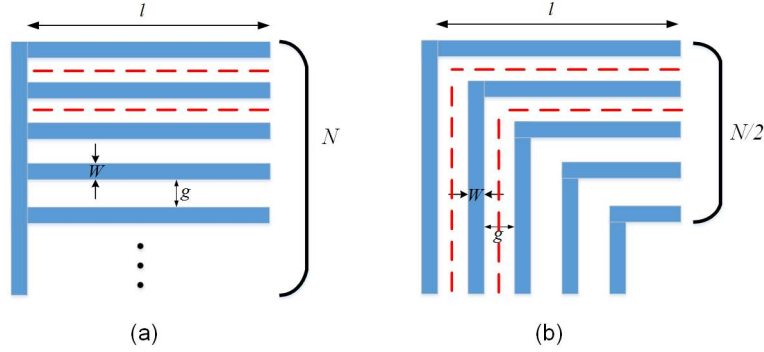


FIGURE 3. Calculation of the total parallel metallic strip length for (a) NSRR, and (b) B-NSRR.

The calculation of total parallel strip length for NSRR is straightforward. There are N parallel metallic strips, and $N - 1$ gaps in between. Therefore, total parallel strip length $l_{tot,NSRR}$ is given as:

$$l_{tot,NSRR} = \sum_{k=1}^{N-1} l = (N - 1)l \quad (1)$$

where l is the length of each strip. For B-NSRR, the midsection paths shown in Figure 3(b) make a 90° bend and have a varying size. The total parallel metal length $l_{tot,BNSRR}$ is then calculated as:

$$\begin{aligned}
l_{tot, BNSRR} &= 2 \times 2 [(l - g/2) + (l - g - w - g/2) + (l - 2g - 2w - g/2) + \dots] \\
&= \sum_{k=1}^{N/2-1} 4[l - (k - 1/2)g - (k - 1)w]
\end{aligned}$$

where W is the strip width and g is the gap between the strips. The summation is made from the first gap until the $(N/2 - 1)^{\text{th}}$ gap, which has the path with smallest length. The result is multiplied with 2 to include the 90° bend portion and further again with 2 due to horizontal symmetry of the structure. Calculated variations of total parallel metallic strip length with the strip number N for the two geometries are presented in Figure 4. Here, the parameter values are selected as $w = g = 0.194$ mm and $l = 4.61$ mm. The comparison of $l_{tot, NSRR}$ and $l_{tot, BNSRR}$ is important, since maximizing the total parallel metallic strip length implies maximizing C_s , which in turn increases the sensitivity of the structure. It can be observed from Figure 4 that the advantage of the B-NSRR is clear for the whole range of N and increases as N is increased before saturating a little bit. Therefore, it can be expected that the B-NSRR yields a higher gap capacitance.

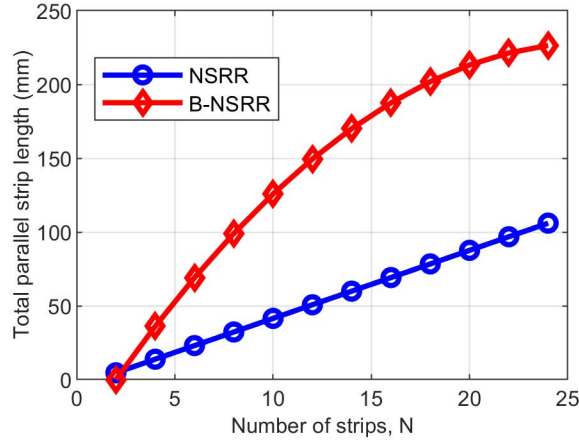


FIGURE 4. Variation of total parallel metallic strip length with strip number N for NSRR and B-NSRR.

For displacement sensing, the B-NSRR structure can also be split into two symmetric parts to form a modified B-NSRR geometry, as illustrated in Figure 1(d). The surface current densities induced on the modified NSRR and B-NSRR structures for a plane wave excitation are shown in Figure 5(a) and Figure 5(b), respectively. Both of the plots are normalized with respect to the same color scale. Both geometries are observed to have a high current density at their top strips shorted

by the jumper. The current distribution of the NSRR is tapered along the vertical axis, while the B-NSRR has a concentrated current density along the middle strip. The fact that the current density is higher close to the vertical gap in the B-NSRR in comparison to the NSRR can be considered as an important advantage in terms of displacement sensing.

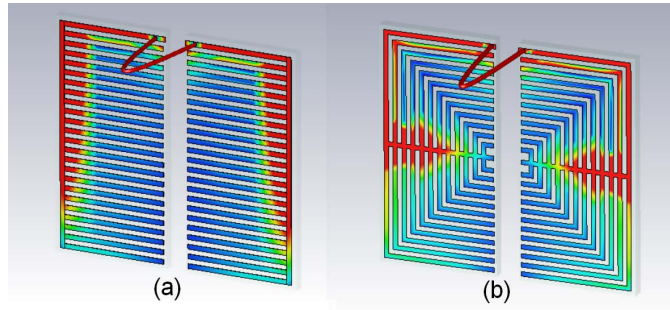


FIGURE 5. Surface current densities induced on the modified (a) NSRR and (b) B-NSRR structures for a plane wave excitation.

3. SRR STRUCTURES AS SENSORS

In this section, the sensing performances of the four SRR-based structures (classic SRR, ESRR, NSRR and B-NSRR) are analyzed with full-wave electromagnetic simulations run on CST Microwave Studio [33]. The designs used in the simulations are illustrated in proportion in Figure 6 and the dimensional parameters of the designs are presented in Table 1. The dielectric material is 0.508-mm-thick Rogers RO4003C with a dielectric constant of 3.55 for all structures. The dimensions are selected such that the resonance frequencies f_{res} of all 4 designs are in 1500–1800 MHz range. Although their f_{res} is around the same range, it can be observed that the ESRR design that corresponds to this frequency has the biggest size. The 3-ring SRR geometry has the second biggest size, while the NSRR and B-NSRR designs have a significantly more compact footprint.

The quality factor (Q) is an important metric for any resonating structure since it is an expression of the ratio of the stored energy to the loss. Therefore, the higher the Q , the better the sensitivity. In order to assess the quality factor of each SRR variant, each structure is excited by a plane wave, and its far-field reflection spectrum is analyzed. It is possible to look at either the absorption cross section (ACS) or the radar cross section (RCS), both of which yield a peak at the resonance frequency of the SRR. Here, we choose to compare the RCS for each structure. In Figure 7, the radar cross sections of each SRR variant with the design parameters given in Table 2 are compared. It can be understood that the B-NSRR yields the highest Q , the ESRR and the SRR come second and third, respectively, while

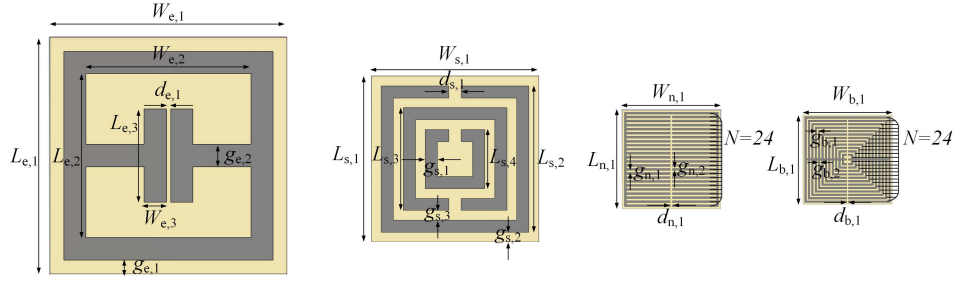


FIGURE 6. ESRR, SRR, NSRR and B-NSRR sensor designs used in this work (shown with a true proportion) with dimension parameters.

TABLE 1. Values of the dimensional parameters of sensors shown in Figure 6.

ESRR		SRR		NSRR		B-NSRR	
$W_{e,1}$	27.1 mm	$W_{s,1}$	18.9 mm	$W_{n,1}$	11.2 mm	$W_{b,1}$	10.2 mm
$W_{e,2}$	18.8 mm	$L_{s,1}$	18.9 mm	$L_{n,1}$	11.2 mm	$L_{b,1}$	10.2 mm
$W_{e,3}$	2.55 mm	$L_{s,2}$	16.7 mm	$d_{n,1}$	0.229 mm	$d_{b,1}$	0.194 mm
$L_{e,1}$	27.1 mm	$L_{s,3}$	11.7 mm	$g_{n,1}$	0.229 mm	$g_{b,1}$	0.194 mm
$L_{e,2}$	18.8 mm	$L_{s,4}$	6.73 mm	$g_{n,2}$	0.229 mm	$g_{b,2}$	0.194 mm
$L_{e,3}$	10.7 mm	$d_{s,1}$	1.40 mm	N	24	N	24
$d_{e,1}$	0.478 mm	$g_{s,1}$	1.37 mm				
$g_{e,1}$	1.59 mm	$g_{s,2}$	1.11 mm				
$g_{e,2}$	2.55 mm	$g_{s,3}$	1.11 mm				

the NSRR provides the smallest Q . It is an interesting fact which shows that the increased capacitance and inductance due to elongation of the strips is more effective in increasing Q than having a higher number of strips (N).

TABLE 2. Quality factor (Q) values for the SRR, ESRR, NSRR and B-NSRR designs.

	Q
SRR	38.7
ESRR	40.3
NSRR	20.9
B-NSRR	80.5

The SRR-based designs are first employed as moisture content sensors in this form, where the decrease of f_{res} is tracked when the water content of the dielectric slab placed behind the structure is gradually increased. The dielectric material loading the sensor mimics an oak tree trunk, whose relative permittivity and loss tangent values measured at different moisture content levels are presented in [34].

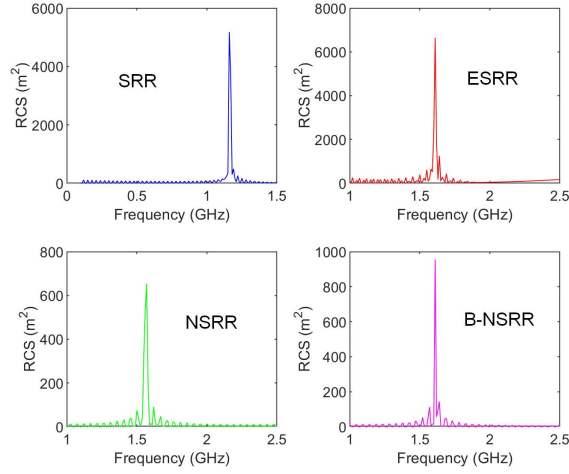


FIGURE 7. Comparison of RCS for SRR, ESRR, NSRR and B-NSRR for the designs whose parameters are given in Table 7.

The NSRR was employed as a moisture content (MC) sensor in [31], where a sensitivity of 1.1 MHz/%MC was demonstrated. Here, a comparison is made between the NSRR, B-NSRR and other SRR variants, and the results are displayed in Figure 8(a). The nonlinear decrease in f_{res} is evident for all structures. Sensitivity metric of the MC sensor can be defined as the average resonance frequency shift per MC change. The frequency shifts Δf_{res} can best be understood by subtracting the f_{res} obtained when MC is zero from all resonance frequencies, which is presented in Figure 8(b). It is observed that the ESRR yields the highest sensitivity with around 275 MHz shift for 90% MC change while the classic SRR and NSRR follow next. B-NSRR design has the lowest Δf_{res} , which is around 170 MHz. These results can be expected since moisture content sensing depends on variation of complex permittivity of the medium loading the SRR-based sensors, and it is inevitably proportional to the dimensions of the structures.

Although they can also be exploited in permittivity-based sensing applications, the real strength of the NSRR and B-NSRR lies in the measurement of one-dimensional strain and displacement, since the structure geometry is optimized especially for this purpose. The variation of C_{gap} with d yields a high sensitivity to mechanical changes occurring in the horizontal axis, which take place either as a high increase or drop in f_{res} . The variation of f_{res} with the gap parameter d is displayed in Figure 9(a), and the frequency shifts Δf_{res} for this case are presented in Figure 9(b). Here, only the results for ESRR, NSRR and B-NSRR are shown, since the classic SRR geometry is not suitable for measurement of relative displacement. All the remaining geometries are optimized for sensing horizontal displacement,

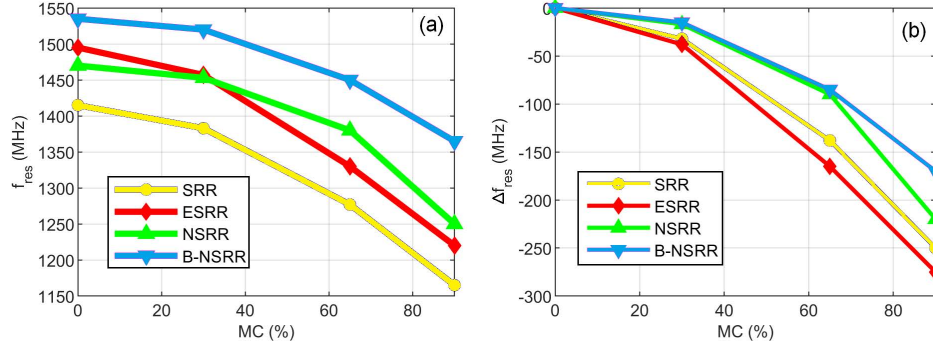


FIGURE 8. (a) Variation of f_{res} with moisture content for an oak sample, (b) the frequency shifts Δf_{res} .

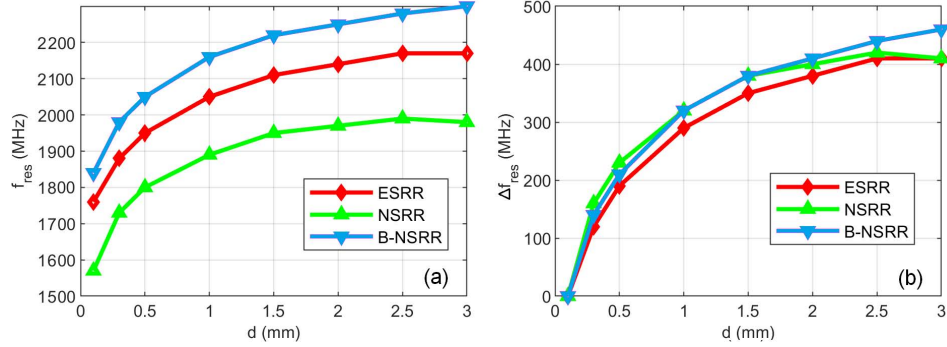


FIGURE 9. (a) Variation of f_{res} with the gap parameter d , (b) the frequency shifts Δf_{res} .

due to the presence of a small gap between the metallic parts. Similar to the modification procedure of the NSRR and B-NSRR, to obtain a displacement sensor, the ESRR structure is also split vertically into two mechanically-independent halves which are electrically shorted at the top and bottom. Sensitivity of the B-NSRR structure is observed to be the highest among all three structures, and it is around $450 \text{ MHz}/3 \text{ mm}=150 \text{ MHz}/\text{mm}$, while the other two are around $400 \text{ MHz}/3 \text{ mm}=133 \text{ MHz}/\text{mm}$. Although B-NSRR is the most compact structure, it also yields the highest displacement sensitivity, which shows its potential as a sensor.

4. CONCLUSION

We present a novel split-ring resonator structure called the bended nested splitting resonator (B-NSRR), which is primarily optimized for applications such as

moisture content, displacement or strain sensing. The structure is a variant of the previously developed NSRR geometry, and similarly, incorporates a high number of metallic strips, enabling better sensitivity and resolution compared to traditional SRR-based structures. Moreover, it offers a way to obtain much more compact designs, which is important in many applications. The sensitivity of the present NSRR structure is enhanced even more by introducing 90° bends on the strips, which leads to an increase in the total parallel metallic length, which in turn boosts the capacitance between the parallel strips. This way, better enhancement of fields and further miniaturization of the NSRR are achieved. Performance of the B-NSRR structure as a sensor of moisture content and relative displacement is compared to that of other SRR-based variants and it is shown that the B-NSRR structure can be utilized for both applications. However, it is observed to be the best option in displacement sensing among all SRR variants since it enables both a more sensitive and a more compact design.

Declaration of Competing Interests The author declares no known competing interests.

REFERENCES

- [1] Smith, D. R., Padilla, W. J., Vier, D. C., Nemat-Nasser, S. C., Schultz, S., Composite medium with simultaneously negative permeability and permittivity, *Phys. Rev. Lett.*, 84 (18) (2000), 4184–4187, <https://doi.org/10.1103/PhysRevLett.84.4184>.
- [2] Shelby, R. A., Smith, D. R., Schultz, S., Experimental verification of a negative index of refraction, *Science*, 292 (5514) (2001), 77–79, <https://doi.org/10.1126/science.1058847>.
- [3] Shelby, R. A., Smith, D. R., Nemat-Nasser, S. C., Schultz, S., Microwave transmission through a two-dimensional, isotropic, left-handed metamaterial, *Appl. Phys. Lett.*, 78 (4) (2001), 489–491, <https://doi.org/10.1063/1.1343489>.
- [4] Pendry, J. B., Negative refraction makes a perfect lens, *Phys. Rev. Lett.*, 85 (18) (2000), 3966–3969, <https://doi.org/10.1103/PhysRevLett.85.3966>.
- [5] Enoch, S., Tayeb, G., Sabouroux, P., Guerin, N., Vincent, P., A metamaterial for directive emission, *Phys. Rev. Lett.*, 89 (21) (2002), 213902, <https://doi.org/10.1103/PhysRevLett.89.213902>.
- [6] Erentok, A. and Luljak, P. L. and Ziolkowski, R. W., Characterization of a volumetric metamaterial realization of an artificial magnetic conductor for antenna applications, *IEEE Trans. Antennas Propag.*, 53 (1) (2005), 160-172, <https://doi.org/10.1109/TAP.2004.840534>.
- [7] Schurig, D., Mock, J. J., Justice, B. J., Cummer, S. A., Pendry, J. B., Starr, A. F., Smith, D. R., Metamaterial electromagnetic cloak at microwave frequencies, *Science*, 314 (5801) (2006), 977–980, <https://doi.org/10.1126/science.1133628>.
- [8] Engheta, N., An idea for thin subwavelength cavity resonators using metamaterials with negative permittivity and permeability, *IEEE Antennas Wireless Propag. Lett.*, 1 (2002), 10-13, <https://doi.org/10.1109/LAWP.2002.802576>.
- [9] Antoniadou, M. A., Eleftheriades, G. V., Compact linear lead/lag metamaterial phase shifters for broadband applications, *IEEE Antennas Wireless Propag. Lett.*, 2 (2003), 103-106, <https://doi.org/10.1109/LAWP.2003.815280>.
- [10] Falcone, F., Lopetegi, T., Baena, J. D., Marques, R., Martin, F., Sorolla, M., Effective negative-epsilon stopband microstrip lines based on complementary split

- ring resonators, *IEEE Microw. Wireless Compon. Lett.*, 14 (6) (2004), 280-282, <https://doi.org/10.1109/LMWC.2004.828029>.
- [11] Antoniadou, M. A., Eleftheriades, G. V., A broadband Wilkinson balun using microstrip metamaterial lines, *IEEE Antennas Wireless Propag. Lett.*, 4 (2005), 209-212, <https://doi.org/10.1109/LAWP.2005.851005>.
- [12] Ziolkowski, R. W., Kipple, A. D., Application of double negative materials to increase the power radiated by electrically small antennas, *IEEE Trans. Antennas Propag.*, 51 (10) (2003), 2626-2640, <https://doi.org/10.1109/10.1109/TAP.2003.817561>.
- [13] Chen, T., Li, S., Sun, H., Metamaterials application in sensing, *Sensors*, 12 (3) (2012), 2742-2765, <https://doi.org/10.3390/s120302742>.
- [14] Lee, H.-J., Lee, J.-H., Moon, H.-S., Jang, I.-S., Choi, J.-S., Yook, J.-G., Jung, H.-I., A planar split-ring resonator-based microwave biosensor for label-free detection of biomolecules, *Sens. Actuators, B*, 169 (2012), 26-31, <https://doi.org/10.1016/j.snb.2012.01.044>.
- [15] Al-Naib, I. A. I., Jansen, C., Koch M., Thin-film sensing with planar asymmetric metamaterial resonators, *Appl. Phys. Lett.*, 93 (8) (2008), 083507, <https://doi.org/10.1063/1.2976636>.
- [16] Melik, R., Unal, E., Perkgoz, N. K., Puttlitz, C., Demir, H. V., Metamaterial based telemetric strain sensing in different materials, *Opt. Express*, 18 (5) (2010), 5000-5007, <https://doi.org/10.1364/OE.18.005000>.
- [17] Tian, X., Lee, P. M. Tan, Y. J., Wu, T. L. Y., Yao, H., Zhang, M., Li, Z., Ng, K. A., Tee, B. C. K., Ho, J. S., Wireless body sensor networks based on metamaterial textiles, *Nat. Electron.*, 2 (6) (2019), 243-251, <https://doi.org/10.1038/s41928-019-0257-7>.
- [18] Ekmekci, E., Turhan-Sayan, G., Multi-functional metamaterial sensor based on a broad-side coupled SRR topology with a multi-layer substrate, *Appl. Phys. A: Mater. Sci. Process.*, 110 (2013), 189-197, <https://doi.org/10.1007/s00339-012-7113-1>.
- [19] Pendry, J.B., Holden, A.J., Robbins, D.J., Stewart, W.J., Magnetism from conductors and enhanced nonlinear phenomena, *IEEE Trans. Microw. Theory Tech.*, 47 (11) (1999), 2075-2084, <https://doi.org/10.1109/22.798002>.
- [20] Engheta, N., Ziolkowski, R. W., *Electromagnetic Metamaterials: Physics and Engineering Explorations*, Wiley, Hoboken, N.J., 2006.
- [21] Padilla, W. J., Aronsson, M. T., Highstrete, C., Lee, M., Taylor, A. J., Averitt, R. D., Electrically resonant terahertz metamaterials: Theoretical and experimental investigations, *Phys. Rev. B: Condens. Matter*, 75 (4) (2007), 041102, <https://doi.org/10.1103/PhysRevB.75.041102>.
- [22] Zhang, J., Tian, G. Y., Marindra, A. M. J., Sunny, A. I., Zhao, A. B., A Review of Passive RFID Tag Antenna-Based Sensors and Systems for Structural Health Monitoring Applications, *Sensors*, 17 (2) (2017), 265, <https://doi.org/10.3390/s17020265>.
- [23] Melik, R., Unal, E., Perkgoz, N.K., Santoni, B., Kamstock, D., Puttlitz, C., Demir, H.V., Nested metamaterials for wireless strain sensing, *IEEE J. Sel. Topics Quantum Electron.*, 16 (2) (2010), 450-458, <https://doi.org/10.1109/JSTQE.2009.2033391>.
- [24] Ozbey, B., Unal, E., Ertugrul, H., Kurc, O., Puttlitz, C. M., Erturk, V. B., Altintas, A., Demir, H. V., Wireless displacement sensing enabled by metamaterial probes for remote structural health monitoring, *Sensors*, 14 (1) (2014), 1691-1704, <https://doi.org/10.3390/s140101691>.
- [25] Ozbey, B., Demir, H. V., Kurc, O., Erturk, V. B., Altintas, A., Wireless measurement of elastic and plastic deformation by a metamaterial-based sensor, *Sensors*, 14 (10) (2014), 19609-19621, <https://doi.org/10.3390/s141019609>.
- [26] Ozbey, B., Demir, H. V., Kurc, O., Erturk, V. B., Altintas, A., Wireless sensing in complex electromagnetic media: Construction materials and structural monitoring, *IEEE Sensors J.*, 15 (10) (2015), 5545-5554, <https://doi.org/10.1109/JSEN.2015.2441555>.

- [27] Ozbey, B., Erturk, V. B., Demir, H. V., Altintas, A., Kurc, O., A wireless passive sensing system for displacement/strain measurement in reinforced concrete members, *Sensors*, 16 (4) (2016), 496, <https://doi.org/10.3390/s16040496>.
- [28] Ozbey, B., Range extension in coupling-based wireless passive displacement sensors for remote structural health monitoring, *IEEE Sensors J.*, 22 (21) (2022), 20268-20275, <https://doi.org/10.1109/JSEN.2022.3206475>.
- [29] Ozbey, B., Ertürk, V. B., Kurc, O., Altintas, A., Demir, H. V., Multi-point single-antenna sensing enabled by wireless nested split-ring resonator sensors, *IEEE Sensors J.*, 16 (21) (2016), 7744–7752, <https://doi.org/10.1109/JSEN.2016.2604020>.
- [30] Ozbey, B., Wireless surface strain mapping by passive electromagnetic resonators, *IEEE Sensors J.*, 23 (10) (2023), 10370-10377, <https://doi.org/10.1109/JSEN.2023.3264948>.
- [31] Ozbey, B., Eibert, T. F., Wireless non-destructive moisture content characterization of trees by highly-sensitive compact resonating probes, *IEEE Sensors J.*, 21 (5) (2021), 6125–6132, <https://doi.org/10.1109/JSEN.2020.3043304>.
- [32] Ozbey, B., Altintas, A., Demir, H. V., Ertürk, V. B., An equivalent circuit model for nested split-ring resonators, *IEEE Trans. Microw. Theory Tech.*, 65 (10) (2017), 3733–3743, <https://doi.org/10.1109/TMTT.2017.2699650>.
- [33] Dassault Systemes, CST Studio Suite, Vélizy-Villacoublay, France, 2019.
- [34] James, W. L., Dielectric Properties of Wood and Hardboard: Variation with Temperature, Frequency, Moisture Content, and Grain Orientation. Department of Agriculture, Forest Service, Forest Products Laboratory, 1975.